Supporting Information

Hare et al. 10.1073/pnas.1109322108

SI Results

Testing for Action Value Coding in Motor Cortex. Activity in both motor cortices increased as a function of the reward obtained by the selected action [i.e., the left motor cortex (lMC) positively correlated with the right value and the right motor cortex (rMC) positively correlated with the left value; $P < 0.05$, corrected] (Table S11).

Note, however, that lMC and rMC did not meet the criteria for the encoding of action values (1, 2), which is defined as a signal that encodes the value of an action regardless of whether it is chosen. Post hoc tests showed that, when the opposite response was chosen, lMC and rMC were not significantly correlated with right [$t_{(18)} = 1.21$, not significant (n.s.)] or left values ($t_{(18)} = -0.09$, n.s.), respectively.

Differences Between Neural Drift Diffusion Model Predictions of Total Activity in Comparator Regions and Difficulty Measures. Although these two measures are highly correlated, there are two important differences between them, which allows us to test which of the two parametric regressors fits better with the patterns of activity found in areas like dorsal medial prefrontal cortex (dmPFC) and intraparietal sulcus (IPS).

First, our neural drift diffusion model (nDDM) model predicts greater activity in comparator regions during error than correct trials (Fig. 2*D*), whereas the measure of difficulty does not differentiate between the two trial types. Here, we define an error trial as one in which the liquid of lower value is chosen. This greater activity in error than correct trials arises as a function of the noise and mutual inhibition parameters of the nDDM model.

Second, the difficulty measure is a simple linear function of the difference in values, whereas the activity predicted by the nDDM is monotonically related to the difference in values but not perfectly linear (Fig. 2*D*). This nonlinearity is present even when considering correct and error trials separately.

Motivated by these differences, we carried out a post hoc Bayesian model selection (3) in dmPFC, dorsolateral prefrontal cortex (dlPFC), and IPS to test whether the total activity measure from the nDDM or the difficulty measure best explained activity in these regions. We used the exceedance probability (EP; the probability that a given model is more likely than any other model in the comparison set given the group data) as our metric for model comparison. The EP of the nDDM model was greater than the difficulty model in all four regions (dmPFC EP = 0.99, dlPFC EP = 0.58, lIPS EP = 0.98, and rIPS EP = 0.94), indicating that the nDDM provided a better fit to activity in these areas than the difficulty measure, especially in dmPFC and IPS.

We ran an additional model comparison to determine whether the nDDM predictions were a better fit to blood oxygen level-dependent (BOLD) signals in dmPFC and IPS than difficulty, even when the distinction between correct and error trials was removed from the parametric regressor. To create this regressor, we assigned the parametric value of all trials as if they were correct. The all correct nDDM parametric regressor fit the BOLD signal better than difficulty (EP > 90%) in all regions of interest. However, the original nDDM regressor is also more likely than the all correct nDDM regressor (EP > 90%) in all regions of interest, indicating that both the shape of the curve and separation between correct and error trials are important factors in the fit to the BOLD signal.

There is also a previous body of literature suggesting that activity in the ventral parts of dmPFC, particularly in the anterior cingulate cortex (ACC), plays a role in resolving response conflict and error monitoring in a variety of tasks (4, 5). Although our results are not fundamentally incompatible with a role for ACC in error monitoring or response conflict in other paradigms, neither role is likely to explain the dmPFC activity in the current study. There are several reasons for this finding. First, the area of dmPFC identified here is more dorsal than the areas of ACC that have generally been associated with these alternative signals in previous studies. Second, response conflict in our paradigm would be the same as the choice difficulty measure discussed above. Third, error monitoring is also an unlikely function for dmPFC in our experiment, because we see the dmPFC become active well before the response (potentially an error) has been made.

SI Materials and Methods

Additional Stimuli and Task Details. Subjects abstained from all liquids for 3 h before the experiment. Before entering the scanner, subjects were asked to consume three saltine crackers to increase their level of thirst and were also given one saltine cracker to eat between the four functional runs to maintain thirst. Thirst ratings were obtained before each functional run to confirm that subjects remained thirsty throughout the task. A different colored shape represented each flavor (apple, grape, fruit punch, and water), with the number of shapes on the screen indicating the amount of liquid (1 = 0.2 mL, 2 = 0.45 mL, or 3 = 0.7 mL). If the subject failed to respond within 1.5 s after the response prompt appeared, an option was selected at random. Stimulus presentation, response recording, and liquid delivery were controlled using Cogent 2000 software (Wellcome Department of Imaging Neuroscience).

Liquid Delivery. Electronic syringe pumps located in the scanning control room delivered each liquid to the subject through ~10 m polyethylene tubing and a perfusion manifold. The perfusion manifold allowed four incoming tubes to be connected to one output tube with a minimum of dead space to avoid mixing the liquids. The subjects held the output tube between their lips like a straw while lying in the supine position inside the MRI scanner. Visual stimuli were presented using an overhead mirror and projection system.

Value of Liquid Rewards. We determined the subjective value of each liquid reward option using the individual's pattern of choices. The value of each flavor–amount combination was calculated using the equation $V = F \times A$, where V is the value of the option, F is the frequency with which that flavor was selected regardless of the amount offered, and A is the amount of liquid offered. All of the other value signals used in the analysis were derived from this basic calculation. In particular, the stimuli value (SV) for each trial was equal to the sum of the values for the available options (left value + right value). Action value left (right) was equal to the left (right) value. Chosen value (CV) was equal to the value of the chosen option, whereas nonchosen value (NCV) was equal to the value of the nonchosen option.

nDDM Estimation Procedure. The nDDM model assumes that the comparator system contains two identical pools of neurons: one encoding the relative value signal for left (i.e., value of left minus value of right) and one encoding the relative value signal for right (i.e., value of right minus value of left). The model also assumes that activity in each of the pools commences at a zero level and that each of them changes after a Gaussian Markovian process similar to the one for the DDM, except that they are not allowed to go below zero at any point during the decision process. Finally, the model assumes

that a choice is made in favor of its respective option when one of the two pools reaches a prespecified threshold level of activity and that the two pools dynamically inhibit each other.

We calibrated the model to the psychometric group choice data by simulating the model 5,000 times with different parameter sets and selecting the parameters that maximized the fit between the simulated and actual choice curves. Maximal fit was evaluated using a sum of square deviations criterion, including a weighting term for each level of $|V_L - V_R|$ that was inversely proportional to its frequency in the dataset. This calculation was done by searching among combinations of the following free parameters: mean and SD of the integration slope (d), SD of the Gaussian noise (η), and inhibition strength (θ). The psychometric curve for the best-fitting set of parameters ($d = 0.009 \pm 0.005$, $\eta = 0 \pm 0.035$, $\theta = 0.2$) is shown in Fig. 2*C*. We used the group choice data, because it leads to less noisy choice curves and therefore, generated more reliable estimates of the parameters of the nDDM.

We then used this set of parameters to estimate the distributions of total activity in both pools of comparator neurons by simulating the model 5,000 times for each combination of value differences. Total activity is defined to be as the sum of instantaneous levels of activity in both pools of neurons from stimulus onset to choice. Fig. 2*D* depicts summary statistics for the resulting distributions for both correct and error trials. The value of total activity in each trial predicted by the model is referred to as M_{out}.

We note one caveat to applying the nDDM to this dataset. Ideally, the experiment would have had free reaction times, which would have helped us to estimate the nDDM parameters more precisely, because the model makes predictions for both the accuracy and reaction time of choices. Because reaction time data are not available in our design, we fitted the nDDM using only the choice data. The lack of reaction time data likely introduces noise in our parameter estimates for the model and thus, reduces our ability to identify comparator regions using fMRI, but it does not introduce any systematic biases in our analyses.

Functional MRI Data Acquisition. The functional imaging was conducted using a Siemens 3.0 Tesla Trio MRI scanner. We acquired gradient echo T2*-weighted echoplanar images (EPIs) with BOLD contrast. To optimize functional sensitivity in the orbitofrontal cortex (OFC), we used a tilted acquisition in an oblique orientation of 30° to the anterior commissure–posterior commissure line (6). In addition, we used an eight-channel phased array coil that yields a 40% signal increase in signal in the OFC over a standard head coil. Each volume comprised 48 axial slices collected in an interleaved-ascending manner. Data were collected in four sessions (209 volumes, ~11 min). The imaging parameters were echo time, 30 ms; field of view, 192 mm; in-plane resolution and slice thickness, 3 mm; repetition time, 3 s. Whole-brain, high-resolution T1-weighted structural scans ($1 \times 1 \times 1$ mm) were acquired from the 20 subjects and coregistered with their mean EPI images; they were averaged together to permit anatomical localization of the functional activations at the group level.

Functional MRI Data Preprocessing. Image analysis was performed using SPM8 (Wellcome Department of Imaging Neuroscience). Images were corrected for slice acquisition time within each volume, motion-corrected, spatially normalized to the standard Montreal Neurological Institute EPI template, and spatially smoothed using a Gaussian kernel with a full width at one-half maximum of 8 mm. Intensity normalization and high-pass temporal filtering (using a filter width of 128 s) were also applied to the data.

General Linear Models. We estimated the following general linear model of BOLD responses to identify regions reflecting stimulus values, action values, and motor responses. This process was done in three steps.

First, for each individual, we estimated a general linear model (GLM) with first-order autoregression and the following nine indicator functions: R1, initial stimulus screen; R2, choice response period (CR); R3, left button press; R4, right button press; R5, juice delivery; R6–9, presence of each preference ranked juice (based on each subject's choices) on the stimulus screen. The stimulus screen, juice delivery, and preference ranked indicators were modeled as events with 1-s durations. The CR period was modeled as an event with duration equal to the elapsed time between the onset of the choice screen and the button press on that trial (5–9.5 s). Left and right button presses were modeled with durations equal to the reaction time as measured by the time elapsed between the appearance of the response screen and the button press. In addition to the nine indicator functions, the model included four parametric regressors: (*i*) choice screen × SV, (*ii*) CR × left V, (*iii*) CR × right V, and (*iv*) juice delivery × CV. The model also included session constants and motion parameters as regressors of no interest.

Second, we calculated first-level, single-subject contrasts for each of the four parametric regressors listed above.

Third, we calculated second-level group contrasts using one-sample t tests on the single-subject contrasts. We carried out whole-brain corrections for multiple comparisons at the cluster level. Details of the correction for each contrast can be found in Tables S1–S11. Small-volume correction for the ventromedial prefrontal cortex (vmPFC) was conducted within a 10-mm sphere centered on the vmPFC coordinates ($x, y, z = -3, 42, -6$) from the work by Chib et al. (7).

We estimated a second GLM to identify regions reflecting the output of our nDDM model. This model included the same indicator functions as the first GLM and the following parametric regressors: (*i*) choice screen × SV, (*ii*) CR × M_{out}, and (*iii*) juice delivery × CV. All omitted details are as detailed.

Post Hoc Analyses. To determine if stimulus location (left vs. right), choice (chosen vs. nonchosen), or identity (liquid 1–4) affected its association with vmPFC activity, we computed three additional GLMs. All of these GLMs included the same three indicator functions of (R1) choice screen, (R2) response screen, and (R3) juice delivery. The location model included parametric modulators for left V and right V for each indicator function. The choice model included parametric modulators for CV and NCV for each indicator function. There was little correlation between left value and right value (mean $r = -0.187$) or CV and NCV (mean $r = 0.183$). The identity model included parametric modulators for the value of each liquid for each indicator function. Liquid values were set to zero on trials where they were not offered.

First-level, single-subject contrasts were created for the parametric modulators left V, right V, chosen V, nonchosen V, and the value of each liquid at the time of choice screen onset. These single-subject contrast values were then averaged across all voxels shown in Fig. 3*A* and compared using paired t tests.

To test whether activity in dmPFC, dlPFC, and Par was more associated with M_{out} or difficulty (|left V − right V|), we estimated an additional GLM. This GLM was identical to the second GLM except that the parametric modulator for M_{out} from the previous model was replaced with |left V − right V|.

Post Hoc Comparison of Fits for nDDM and Difficulty GLMs. We created functional masks in dmPFC, dlPFC, and left and right Par from all voxels in those regions correlating with M_{out} and difficulty (conjunction threshold $P < 0.005$, uncorrected for each contrast). Next, we reestimated both GLMs using the Bayesian first-level estimation techniques incorporated into SPM8 and previously described in detail in the work by Penny et al. (8). Last, we used

a random effects Bayesian model selection procedure to determine exceedance probabilities that indicated whether the M_{out} or difficulty models provided a better fit to the data in each of the three regions. A brief description of this method is given in *Materials and Methods* on dynamic causal modeling, and additional details can be found in two recent papers (3, 9).

Dynamic Causal Modeling Description. For all 20 models tested, the driving inputs to all regions were assigned based on the results from the univariate GLMs and were not mean-centered (i.e., the fixed coupling parameters represent connectivity in the absence of task stimulation). Those inputs included five inputs: (*i*) an input of constant magnitude into vmPFC and dlPFC during stimulus presentation, (*ii*) an input to vmPFC during stimulus presentation proportional to the sum of the stimulus values, (*iii*) an input into dmPFC, dlPFC, and bilateral IPS of constant magnitude during the period from stimulus onset to button press for left choices, (*iv*) an input into dmPFC, dlPFC, and bilateral IPS of constant unit magnitude during the period from stimulus onset to button press for right choices, and (*v*) an input of constant value into lMC and rMC at the time of response. Parameter estimates for the inputs to each region are shown in Table S10. In addition, all of the models allowed for the following event-related changes in coupling strength: (*i*) the coupling from vmPFC to dmPFC, dlPFC, and parietal cortex was allowed to be influenced by the onset of the stimulus screen (unmodulated), (*ii* and *iii*) left and right CR periods were allowed to modulate coupling in all existing connections, and (*iv*) button presses were allowed to modulate self-connections in lMC and rMC. To carry out these analyses, we estimated an additional GLM that was identical to the first GLM described in *Materials and Methods* except that the CR period was separated into right and left choice trials, the choice screen was modeled with an indicator function of 2-s duration, and the indicators for each preference-ranked juice were omitted.

Bayesian Model Selection for Dynamic Causal Modeling. We identified the best model using the Bayesian model selection method developed by Stephan et al. (3). Briefly, this technique treats the models as random variables and computes a distribution of the probabilities for all models under consideration. The probabilities can be used to define a multinomial distribution over model space from which the likelihood that a specific model generated the data of a randomly selected subject can be estimated. This procedure permits the computation of the exceedance probability for each model in the comparison set, which measures the probability that each model is the most likely one to be correct. Note that the exceedance probabilities add to one over the comparison set and thus, generally decrease as the number of models considered increases. We posited 20 different models of connectivity involving the seven areas identified above (vmPFC, dmPFC, dlPFC, lMC, rMC, lIPS, and rIPS) and used a Bayesian model selection process to identify the most probable model in the set (Fig. S3). The set of alternative models is described in detail in Tables S5–S10. We specified a large set of models, because given existing data, we did not have strong priors about the exact pattern of connectivity in the network. The set of models considered included the model depicted in Fig. 4 and most variations where vmPFC, dlPFC, and IPS are disconnected from sets of one or two other regions, including motor cortex.

Bayesian Parameter Averaging. Here, we present the equations underlying the Bayesian parameter averaging method that we used to make inferences about the modulatory dynamic causal modeling parameters at the group level. As stated in the work by Kasess et al. (10) and in other works (11, 12), this procedure treats the posterior distribution for one subject as the prior for the next subject. The process continues up to the *n*th subject, resulting in the following expression (**S1**):

$$\begin{aligned} p(\theta|y_1,\ldots,y_N) &\propto p(\theta)\prod_{i=1}^{N} p(y_i|\theta) \\ &\propto p(\theta|y_1)\prod_{i=2}^{N} p(y_i|\theta) \\ &\propto p(\theta|y_1,\ldots,y_{N-1})\prod_{i=N}^{N} p(y_i|\theta) \end{aligned} \quad \textbf{[S1]}$$

Under Gaussian assumptions about the densities, which is the case in dynamic causal modeling, the procedure can be simplified using a reduced form, where subject-specific conditional parameter densities are weighted by their precision and summed across subjects (Eq. **S2**):

$$\mu = \Lambda^{-1}\sum_{i=1}^{N}\Lambda_i\mu_i \quad \textbf{[S2]}$$

and (Eq. **S3**)

$$\Lambda = \sum_{i=1}^{N}\Lambda_i \quad \textbf{[S3]}$$

where μ_i is the posterior mean of the *i*th subject and $\Lambda_I = \Sigma_i^{-1}$ is the inverse posterior covariance or precision matrix. The matrix Λ represents not only the precisions of the model parameters (on the diagonal) but also the interdependence of the parameters (off-diagonal elements). The incorporation of the within subjects estimation precision is an advantage of Bayesian parameter averaging over frequentist approaches (e.g., one-sample *t* test) that do not include any measure of within subject variance.

1. Lau B, Glimcher PW (2008) Value representations in the primate striatum during matching behavior. *Neuron* 58:451–463.
2. Wunderlich K, Rangel A, O'Doherty JP (2009) Neural computations underlying action-based decision making in the human brain. *Proc Natl Acad Sci USA* 106: 17199–17204.
3. Stephan KE, Penny WD, Daunizeau J, Moran RJ, Friston KJ (2009) Bayesian model selection for group studies. *Neuroimage* 46:1004–1017.
4. Botvinick MM (2007) Conflict monitoring and decision making: Reconciling two perspectives on anterior cingulate function. *Cogn Affect Behav Neurosci* 7:356–366.
5. Carter CS, van Veen V (2007) Anterior cingulate cortex and conflict detection: An update of theory and data. *Cogn Affect Behav Neurosci* 7:367–379.
6. Deichmann R, Gottfried JA, Hutton C, Turner R (2003) Optimized EPI for fMRI studies of the orbitofrontal cortex. *Neuroimage* 19:430–441.
7. Chib VS, Rangel A, Shimojo S, O'Doherty JP (2009) Evidence for a common representation of decision values for dissimilar goods in human ventromedial prefrontal cortex. *J Neurosci* 29:12315–12320.
8. Penny WD, Trujillo-Barreto NJ, Friston KJ (2005) Bayesian fMRI time series analysis with spatial priors. *Neuroimage* 24:350–362.
9. Rosa MJ, Bestmann S, Harrison L, Penny W (2010) Bayesian model selection maps for group studies. *Neuroimage* 49:217–224.
10. Kasess CH, et al. (2010) Multi-subject analyses with dynamic causal modeling. *Neuroimage* 49:3065–3074.
11. Neumann J, Lohmann G (2003) Bayesian second-level analysis of functional magnetic resonance images. *Neuroimage* 20:1346–1355.
12. Garrido MI, Kilner JM, Kiebel SJ, Stephan KE, Friston KJ (2007) Dynamic causal modelling of evoked potentials: A reproducibility study. *Neuroimage* 36:571–580.

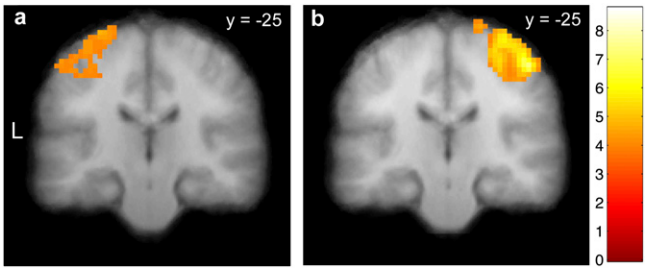

Fig. S1. Motor regions associated with left and right action selection. (*A*) Activity in the left motor cortex was greater when selecting the right juice reward with the right thumb than when selecting the left juice reward with the left thumb ($P < 0.05$, whole-brain corrected). (*B*) Activity in the right motor cortex was greater when selecting the left juice reward with the left thumb than when selecting the right juice reward with the right thumb ($P < 0.05$, whole-brain corrected).

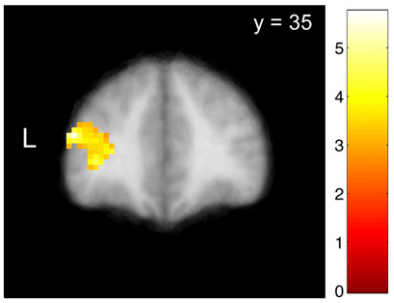

Fig. S2. Area of left dlPFC in which activity was also correlated with the predicted levels of activity generated by the nDDM at $P < 0.05$, whole-brain corrected.

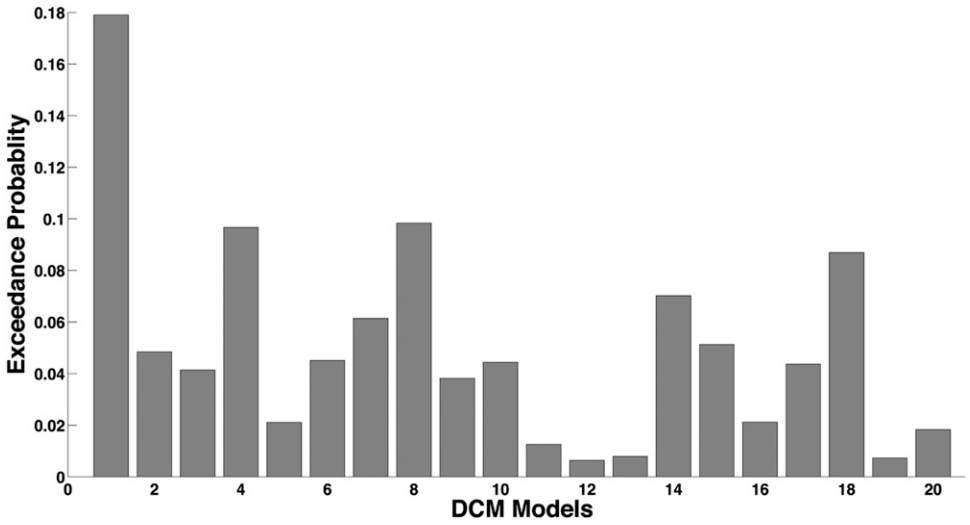

Fig. S3. Exceedance probabilities for the 20 alternative connectivity models. This measure represents the probability that each model is the most likely one to be correct among the set of models tested. The numbers on the *x* axis correspond to the numbering of the models in Table S4. The most probable model (dynamic causal model 1) is shown in Fig. 4 and Tables S5–S10.

Table S1. Regions correlating with stimulus values

Region	BA	Side	Cluster size	*x*	*y*	*z*	*Z* score
Occipital cortex	19/18	B	3,272	−18	−94	13	5.33*
Hippocampus		Left	37	−18	−25	−8	3.94
Hippocampus/amygdala		Right	47	12	−7	−11	3.72
Medial orbitofrontal/anterior cingulate cortex	10	Left	48	−6	44	−5	3.55†
Superior parietal lobule	7	Right	34	21	−70	46	3.37

Height threshold $t = 2.88$; extent threshold = 20 voxels (3 × 3 × 3 mm). BA, Brodmann area.
*The activation survives whole-brain correction for multiple comparisons at the cluster level (height threshold $t = 2.88$, extent = 134 voxels).
†Survives small-volume correction within a 10-mm sphere centered on the vmPFC coordinates ($x, y, z = -3, 42, -6$) from the work of Chib et al. (1).

1. Chib VS, Rangel A, Shimojo S, O'Doherty JP (2009) Evidence for a common representation of decision values for dissimilar goods in human ventromedial prefrontal cortex. *J Neurosci* 29: 12315−12320.

Table S2. Regions reflecting motor responses

Region	BA	Side	Cluster size	*x*	*y*	*z*	*Z* score
Regions showing greater responses for left vs. right responses							
Cerebellum		Left	968	−12	−52	−23	5.4*
Precentral gyrus	6/4/3	Right	1,188	42	−19	67	5.22*
Rolandic operculum/insula	13	Right	100	45	−19	19	3.99
Middle temporal gyrus	21	Left	44	−66	−43	−11	3.36
Putamen		Right	61	27	−10	4	3.3
Regions showing greater responses for right vs. left responses							
Precentral gyrus	4/3/6	Left	749	−45	−34	64	4.33*
Cuneus	18	Right	37	18	−97	7	3.75
Fusiform gyrus	19	Right	29	21	−64	−14	3.60
Cerebellum		Right	47	21	−49	−23	3.35

Height threshold $t = 2.88$; extent threshold = 20 voxels (3 × 3 × 3 mm). BA, Brodmann area.
*The activation survives whole-brain correction for multiple comparisons at the cluster level (height threshold $t = 2.88$, extent = 137 voxels).

Table S3. Regions reflecting the pattern of activity predicted by the DDM implementation

Region	BA	Side	Cluster size	*x*	*y*	*z*	*Z* score
Parietal cortex (IPS)	40/7	Left	483	−30	−70	55	4.27*
Insula	13/47	Left	53	−30	17	4	4.21
Middle/inferior frontal gyrus	46/10	Left	364	−51	35	19	4.17*
Parietal cortex (IPS)	40/7	Right	379	30	−49	40	3.92*
Medial frontal/cingulate gyrus	6/32	Right	193	0	14	58	3.86*
Inferior temporal lobe	37/20	Left	64	−54	−58	−17	3.82
Middle/inferior frontal gyrus	10/46	Right	125	42	41	10	3.77
Anterior cingulate cortex	24	Right	29	0	2	25	3.59
Precentral gyrus	6	Left	37	−45	−4	43	3.57
Lingual gyrus	18	Left	25	−12	−79	−8	3.55
Precentral gyrus	6	Left	32	−60	−10	40	3.47
Cerebellum		Left	95	−33	−67	−38	3.46
Inferior temporal lobe	17/18/19	Right	82	33	−70	−8	3.25
Precuneus	7	Right	23	12	−70	49	3.08
Thalamus		Left	27	−15	−13	13	3.07
Precuneus	7	Left	44	−6	−67	55	2.94
Posterior cingulate cortex	23	Right	20	6	−31	22	2.93

Height threshold $t = 2.88$; extent threshold = 20 voxels (3 × 3 × 3 mm). BA, Brodmann area.
*The activation survives whole-brain correction for multiple comparisons at the cluster level (height threshold $t = 2.88$, extent = 126 voxels).

Table S4. Alternative dynamic causal models tested

Region	*vmPFC* ⇒	*dmPFC* ⇒	*lIPS* ⇒	*rIPS* ⇒	*dlPFC* ⇒	*lMC* ⇒	*rMC* ⇒
DCM 1							
vmPFC	1	1	1	1	1	0	0
dmPFC	1	1	1	1	1	0	0
lIPS	1	1	1	1	1	0	0
rIPS	1	1	1	1	1	0	0
dlPFC	1	1	1	1	1	0	0
lMC	0	1	1	1	1	1	1
rMC	0	1	1	1	1	1	1
DCM 2							
vmPFC	1	0	1	1	1	0	0
dmPFC	0	1	1	1	1	0	0
lIPS	1	1	1	1	1	0	0
rIPS	1	1	1	1	1	0	0
dlPFC	1	1	1	1	1	0	0
lMC	0	1	1	1	1	1	1
rMC	0	1	1	1	1	1	1
DCM 3							
vmPFC	1	1	0	0	1	0	0
dmPFC	1	1	1	1	1	0	0
lIPS	0	1	1	1	1	0	0
rIPS	0	1	1	1	1	0	0
dlPFC	1	1	1	1	1	0	0
lMC	0	1	1	1	1	1	1
rMC	0	1	1	1	1	1	1
DCM 4							
vmPFC	1	1	1	1	0	0	0
dmPFC	1	1	1	1	1	0	0
lIPS	1	1	1	1	1	0	0
rIPS	1	1	1	1	1	0	0
dlPFC	0	1	1	1	1	0	0
lMC	0	1	1	1	1	1	1
rMC	0	1	1	1	1	1	1
DCM 5							
vmPFC	1	1	0	0	0	0	0
dmPFC	1	1	1	1	1	0	0
lIPS	0	1	1	1	1	0	0
rIPS	0	1	1	1	1	0	0
dlPFC	0	1	1	1	1	0	0
lMC	0	1	1	1	1	1	1
rMC	0	1	1	1	1	1	1
DCM 6							
vmPFC	1	1	1	1	1	0	0
dmPFC	1	1	0	0	1	0	0
lIPS	1	0	1	1	1	0	0
rIPS	1	0	1	1	1	0	0
dlPFC	1	1	1	1	1	0	0
lMC	0	1	1	1	1	1	1
rMC	0	1	1	1	1	1	1
DCM 7							
vmPFC	1	1	1	1	1	0	0
dmPFC	1	1	0	0	1	0	0
lIPS	1	1	1	1	1	0	0
rIPS	1	1	1	1	1	0	0
dlPFC	1	1	1	1	1	0	0
lMC	0	1	1	1	1	1	1
rMC	0	1	1	1	1	1	1
DCM 8							
vmPFC	1	1	1	1	1	0	0
dmPFC	1	1	1	1	0	0	0
lIPS	1	1	1	1	1	0	0
rIPS	1	1	1	1	1	0	0
dlPFC	1	0	1	1	1	0	0
lMC	0	1	1	1	1	1	1

Table S4. Cont.

Region	*vmPFC* ⇒	*dmPFC* ⇒	*lIPS* ⇒	*rIPS* ⇒	*dlPFC* ⇒	*lMC* ⇒	*rMC* ⇒
rMC	0	1	1	1	1	1	1
DCM 9							
vmPFC	1	1	1	1	1	0	0
dmPFC	1	1	0	0	0	0	0
lIPS	1	0	1	1	1	0	0
rIPS	1	0	1	1	1	0	0
dlPFC	1	0	1	1	1	0	0
lMC	0	1	1	1	1	1	1
rMC	0	1	1	1	1	1	1
DCM 10							
vmPFC	1	1	1	1	1	0	0
dmPFC	1	1	1	1	1	0	0
lIPS	1	1	1	1	1	0	0
rIPS	1	1	1	1	1	0	0
dlPFC	1	1	1	1	1	0	0
lMC	0	0	1	1	1	1	1
rMC	0	0	1	1	1	1	1
DCM 11							
vmPFC	1	1	1	1	1	0	0
dmPFC	1	1	1	1	1	0	0
lIPS	1	1	1	1	1	0	0
rIPS	1	1	1	1	1	0	0
dlPFC	1	1	1	1	1	0	0
lMC	0	1	0	0	1	1	1
rMC	0	1	0	0	1	1	1
DCM 12							
vmPFC	1	1	1	1	1	0	0
dmPFC	1	1	1	1	1	0	0
lIPS	1	1	1	1	1	0	0
rIPS	1	1	1	1	1	0	0
dlPFC	1	1	1	1	1	0	0
lMC	0	1	0	0	0	1	1
rMC	0	1	0	0	0	1	1
DCM 13							
vmPFC	1	1	1	1	1	0	0
dmPFC	1	1	1	1	1	0	0
lIPS	1	0	1	1	1	0	0
rIPS	1	0	1	1	1	0	0
dlPFC	1	0	1	1	1	0	0
lMC	0	1	0	0	0	1	1
rMC	0	1	0	0	0	1	1
DCM 14							
vmPFC	1	1	1	1	1	0	0
dmPFC	1	1	1	1	1	0	0
lIPS	1	1	1	1	0	0	0
rIPS	1	1	1	1	0	0	0
dlPFC	1	1	0	0	1	0	0
lMC	0	1	1	1	1	1	1
rMC	0	1	1	1	1	1	1
DCM 15							
vmPFC	1	1	0	0	1	0	0
dmPFC	1	1	1	1	1	0	0
lIPS	1	1	1	1	1	0	0
rIPS	1	1	1	1	1	0	0
dlPFC	1	1	1	1	1	0	0
lMC	0	1	1	1	1	1	1
rMC	0	1	1	1	1	1	1
DCM 16							
vmPFC	1	1	1	1	1	0	0
dmPFC	1	1	1	1	1	0	0
lIPS	1	1	1	1	1	0	0
rIPS	1	1	1	1	1	0	0

Table S4. Cont.

Region	*vmPFC* ⇒	*dmPFC* ⇒	*lIPS* ⇒	*rIPS* ⇒	*dlPFC* ⇒	*lMC* ⇒	*rMC* ⇒
dlPFC	1	1	1	1	1	0	0
lMC	0	1	0	1	1	1	1
rMC	0	1	1	0	1	1	1
DCM 17							
vmPFC	1	1	1	1	1	0	0
dmPFC	1	1	1	1	1	0	0
lIPS	1	1	1	1	1	0	0
rIPS	1	1	1	1	1	0	0
dlPFC	1	1	1	1	1	0	0
lMC	0	1	1	1	0	1	1
rMC	0	1	1	1	0	1	1
DCM 18							
vmPFC	1	1	1	1	1	0	0
dmPFC	1	1	1	1	1	0	0
lIPS	1	1	1	1	0	0	0
rIPS	1	1	1	1	0	0	0
dlPFC	1	1	1	1	1	0	0
lMC	0	1	1	1	1	1	1
rMC	0	1	1	1	1	1	1
DCM 19							
vmPFC	1	1	1	1	1	0	0
dmPFC	1	1	1	1	1	0	0
lIPS	1	1	1	1	1	0	0
rIPS	1	1	1	1	1	0	0
dlPFC	1	1	1	1	1	0	0
lMC	0	0	0	0	1	1	1
rMC	0	0	0	0	1	1	1
DCM 20							
vmPFC	1	1	1	1	1	0	0
dmPFC	1	1	0	0	0	0	0
lIPS	1	0	1	0	0	0	0
rIPS	1	0	0	1	0	0	0
dlPFC	1	0	0	0	0	0	0
lMC	0	1	1	1	1	1	1
rMC	0	1	1	1	1	1	1

Connection directionality moves from columns to rows as the arrows indicate. Existing connections are represented by ones, whereas zeros indicate no connection between regions. DCM, dynamic causal modeling.

Table S5. Fixed coupling parameters for the most likely dynamic causal model

	vmPFC ⇒	*dmPFC* ⇒	*lIPS* ⇒	*rIPS* ⇒	*dlPFC* ⇒	*lMC* ⇒	*rMC* ⇒
vmPFC	−1	**0.05** (σ^2 = 0.19e^{-3}; P_c = 1)	**0.06** (σ^2 = 0.18e^{-3}; P_c = 1)	**0.04** (σ^2 = 0.18e^{-3}; P_c = 1)	**0.03** (σ^2 = 0.19e^{-3}; P_c = 0.99)	—	—
dmPFC	**0.03** (σ^2 = 0.18e^{-3}; P_c = 0.99)	−1	**0.05** (σ^2 = 0.16e^{-3}; P_c = 1)	**0.02** (σ^2 = 0.16e^{-3}; P_c = 0.96)	**0.03** (σ^2 = 0.18e^{-3}; P_c = 0.98)	—	—
lIPS	**0.03** (σ^2 = 0.18e^{-3}; P_c = 0.99)	0.01 (σ^2 = 0.18e^{-3}; P_c = 0.8)	−1	0.01 (σ^2 = 0.17e^{-3}; P_c = 0.84)	**0.03** (σ^2 = 0.18e^{-3}; P_c = 0.98)	—	—
rIPS	**0.03** (σ^2 = 0.18e^{-3}; P_c = 0.98)	**0.02** (σ^2 = 0.18e^{-3}; P_c = 0.96)	**0.05** (σ^2 = 0.17e^{-3}; P_c = 1)	−1	**0.02** (σ^2 = 0.18e^{-3}; P_c = 0.96)	—	—
dlPFC	0.02 (σ^2 = 0.17e^{-3}; P_c = 0.89)	**0.02** (σ^2 = 0.18e^{-3}; P_c = 0.95)	**0.03** (σ^2 = 0.16e^{-3}; P_c = 0.98)	0 (σ^2 = 0.17e^{-3}; P_c = 0.61)	−1	—	—
lMC	—	**0.02** (σ^2 = 0.19e^{-3}; P_c = 0.91)	**0.03** (σ^2 = 0.18e^{-3}; P_c = 0.97)	**0.02** (σ^2 = 0.17e^{-3}; P_c = 0.93)	**0.02** (σ^2 = 0.19e^{-3}; P_c = 0.93)	−1	−0.01 (σ^2 = 0.18e^{-3}; P_c = 0.79)
rMC	—	**0.04** (σ^2 = 0.18e^{-3}; P_c = 1)	−0.01 (σ^2 = 0.18e^{-3}; P_c = 0.65)	0 (σ^2 = 0.17e^{-3}; P_c = 0.56)	**0.03** (σ^2 = 0.19e^{-3}; P_c = 0.98)	**−0.02** (σ^2 = 0.18e^{-3}; P_c = 0.94)	−1

Each cell provides statistics for the connection from the column area to the row area. σ^2, sample variance; P, probability that the specified input drives activity in the given region; P_c, probability that the absolute value of the coupling parameter is greater than zero [note that the absolute magnitude of coupling parameters is relative to the driving inputs and will change based on the scale of any parametric modulator (e.g., stimulus value) used as a driving input to the model]; P_m, probability that the coupling parameter is modulated by task condition. The effect size for these parameters should be evaluated relative to the magnitude of the fixed coupling parameters. Parameters with a posterior probability greater than 90% are shown in bold. All values are rounded to two decimals.

Table S6. Modulation of coupling parameters at initial options presentation

	vmPFC ⇒	*dmPFC* ⇒	*lIPS* ⇒	*rIPS* ⇒	*dlPFC* ⇒	*lMC* ⇒	*rMC* ⇒
vmPFC	**0.02** (σ^2 = 0.2e^{-3}; P_m = 0.93)	0 (σ^2 = 0.2e^{-3}; P_m = 0.62)	0 (σ^2 = 0.2e^{-3}; P_m = 0.63)	0 (σ^2 = 0.2e^{-3}; P_m = 0.57)	0 (σ^2 = 0.2e^{-3}; P_m = 0.63)	—	—
dmPFC	**0.02** (σ^2 = 0.19e^{-3}; P_m = 0.93)	0.01 (σ^2 = 0.2e^{-3}; P_m = 0.77)	0 (σ^2 = 0.2e^{-3}; P_m = 0.57)	0 (σ^2 = 0.2e^{-3}; P_m = 0.51)	0.01 (σ^2 = 0.2e^{-3}; P_m = 0.79)	—	—
lIPS	**0.03** (σ^2 = 0.19e^{-3}; P_m = 0.97)	0 (σ^2 = 0.2e^{-3}; P_m = 0.51)	0.02 (σ^2 = 0.2e^{-3}; P_m = 0.89)	0.01 (σ^2 = 0.2e^{-3}; P_m = 0.71)	0.01 (σ^2 = 0.2e^{-3}; P_m = 0.8)	—	—
rIPS	**0.02** (σ^2 = 0.19e^{-3}; P_m = 0.95)	0 (σ^2 = 0.2e^{-3}; P_m = 0.6)	0.01 (σ^2 = 0.2e^{-3}; P_m = 0.76)	0.02 (σ^2 = 0.2e^{-3}; P_m = 0.88)	0.01 (σ^2 = 0.2e^{-3}; P_m = 0.71)	—	—
dlPFC	0 (σ^2 = 0.19e^{-3}; P_m = 0.59)	0 (σ^2 = 0.2e^{-3}; P_m = 0.63)	0 (σ^2 = 0.2e^{-3}; P_m = 0.58)	0 (σ^2 = 0.2e^{-3}; P_m = 0.51)	0.01 (σ^2 = 0.2e^{-3}; P_m = 0.74)	—	—
lMC	—	0 (σ^2 = 0.2e^{-3}; P_m = 0.63)	0 (σ^2 = 0.2e^{-3}; P_m = 0.62)	0 (σ^2 = 0.2e^{-3}; P_m = 0.63)	0.01 (σ^2 = 0.2e^{-3}; P_m = 0.78)	0 (σ^2 = 0.2e^{-3}; P_m = 0.59)	0 (σ^2 = 0.2e^{-3}; P_m = 0.54)
rMC	—	0.01 (σ^2 = 0.2e^{-3}; P_m = 0.74)	0 (σ^2 = 0.2e^{-3}; P_m = 0.58)	0.01 (σ^2 = 0.2e^{-3}; P_m = 0.65)	0.01 (σ^2 = 0.2e^{-3}; P_m = 0.81)	0 (σ^2 = 0.2e^{-3}; P_m = 0.53)	0 (σ^2 = 0.2e^{-3}; P_m = 0.63)

Each cell provides statistics for the connection from the column area to the row area. σ^2, sample variance; P, probability that the specified input drives activity in the given region; P_c, probability that the absolute value of the coupling parameter is greater than zero [note that the absolute magnitude of coupling parameters is relative to the driving inputs and will change based on the scale of any parametric modulator (e.g., stimulus value) used as a driving input to the model]; P_m, probability that the coupling parameter is modulated by task condition. The effect size for these parameters should be evaluated relative to the magnitude of the fixed coupling parameters. Parameters with a posterior probability greater than 90% are shown in bold. All values are rounded to two decimals.

Table S7. Modulation of coupling parameters by choice during the period from stimulus onset to response conditional on left choice

	vmPFC ⇒	*dmPFC ⇒*	*lIPS ⇒*	*rIPS ⇒*	*dlPFC ⇒*	*lMC ⇒*	*rMC ⇒*
vmPFC	**0.02** (σ^2 = 0.19e^{-3}; P_m = 0.92)	0.02 (σ^2 = 0.19e^{-3}; P_m = 0.88)	0.02 (σ^2 = 0.19e^{-3}; P_m = 0.89)	0.01 (σ^2 = 0.19e^{-3}; P_m = 0.86)	0.01 (σ^2 = 0.2e^{-3}; P_m = 0.8)	—	—
dmPFC	0.01 (σ^2 = 0.19e^{-3}; P_m = 0.78)	**0.02** (σ^2 = 0.2e^{-3}; P_m = 0.96)	**0.02** (σ^2 = 0.18e^{-3}; P_m = 0.92)	0.01 (σ^2 = 0.18e^{-3}; P_m = 0.8)	**0.02** (σ^2 = 0.19e^{-3}; P_m = 0.9)	—	—
lIPS	0.01 (σ^2 = 0.19e^{-3}; P_m = 0.83)	0.01 (σ^2 = 0.19e^{-3}; P_m = 0.79)	**0.04** (σ^2 = 0.19e^{-3}; P_m = 0.99)	0.01 (σ^2 = 0.19e^{-3}; P_m = 0.8)	0.01 (σ^2 = 0.19e^{-3}; P_m = 0.84)	—	—
rIPS	0.01 (σ^2 = 0.19e^{-3}; P_m = 0.77)	0.01 (σ^2 = 0.19e^{-3}; P_m = 0.79)	**0.02** (σ^2 = 0.19e^{-3}; P_m = 0.97)	**0.03** (σ^2 = 0.19e^{-3}; P_m = 0.99)	0.01 (σ^2 = 0.19e^{-3}; P_m = 0.77)	—	—
dlPFC	0 (σ^2 = 0.18e^{-3}; P_m = 0.56)	0.01 (σ^2 = 0.19e^{-3}; P_m = 0.73)	0.01 (σ^2 = 0.18e^{-3}; P_m = 0.7)	0 (σ^2 = 0.19e^{-3}; P_m = 0.6)	0.02 (σ^2 = 0.2e^{-3}; P_m = 0.86)	—	—
lMC	—	**−0.03** (σ^2 = 0.19e^{-3}; P_m = 0.97)	**−0.02** (σ^2 = 0.18e^{-3}; P_m = 0.97)	**−0.02** (σ^2 = 0.19e^{-3}; P_m = 0.93)	−0.01 (σ^2 = 0.19e^{-3}; P_m = 0.79)	0.01 (σ^2 = 0.2e^{-3}; P_m = 0.73)	−0.02 (σ^2 = 0.2e^{-3}; P_m = 0.88)
rMC	—	**0.04** (σ^2 = 0.19e^{-3}; P_m = 1)	**0.02** (σ^2 = 0.19e^{-3}; P_m = 0.92)	**0.03** (σ^2 = 0.19e^{-3}; P_m = 0.97)	**0.02** (σ^2 = 0.19e^{-3}; P_m = 0.96)	0.01 (σ^2 = 0.2e^{-3}; P_m = 0.7)	**0.04** (σ^2 = 0.2e^{-3}; P_m = 1)

Each cell provides statistics for the connection from the column area to the row area. σ^2, sample variance; P, probability that the specified input drives activity in the given region; P_c, probability that the absolute value of the coupling parameter is greater than zero [note that the absolute magnitude of coupling parameters is relative to the driving inputs and will change based on the scale of any parametric modulator (e.g., stimulus value) used as a driving input to the model]; P_m, probability that the coupling parameter is modulated by task condition. The effect size for these parameters should be evaluated relative to the magnitude of the fixed coupling parameters. Parameters with a posterior probability greater than 90% are shown in bold. All values are rounded to two decimals.

Table S8. Modulation of coupling parameters by choice during the period from stimulus onset to response conditional on right choice

	vmPFC ⇒	*dmPFC ⇒*	*lIPS ⇒*	*rIPS ⇒*	*dlPFC ⇒*	*lMC ⇒*	*rMC ⇒*
vmPFC	0.02 (σ^2 = 0.19e^{-3}; P_m = 0.89)	**0.02** (σ^2 = 0.19e^{-3}; P_m = 0.93)	**0.03** (σ^2 = 0.19e^{-3}; P_m = 0.98)	0.02 (σ^2 = 0.19e^{-3}; P_m = 0.87)	0.01 (σ^2 = 0.2e^{-3}; P_m = 0.85)	—	—
dmPFC	0.02 (σ^2 = 0.19e^{-3}; P_m = 0.89)	**0.02** (σ^2 = 0.19e^{-3}; P_m = 0.95)	0.02 (σ^2 = 0.18e^{-3}; P_m = 0.87)	0 (σ^2 = 0.18e^{-3}; P_m = 0.55)	0.01 (σ^2 = 0.19e^{-3}; P_m = 0.69)	—	—
lIPS	0.01 (σ^2 = 0.19e^{-3}; P_m = 0.83)	0 (σ^2 = 0.19e^{-3}; P_m = 0.56)	**0.03** (σ^2 = 0.19e^{-3}; P_m = 0.99)	0 (σ^2 = 0.19e^{-3}; P_m = 0.5)	0.01 (σ^2 = 0.19e^{-3}; P_m = 0.68)	—	—
rIPS	0.02 (σ^2 = 0.19e^{-3}; P_m = 0.89)	0.01 (σ^2 = 0.19e^{-3}; P_m = 0.7)	**0.02** (σ^2 = 0.18e^{-3}; P_m = 0.92)	**0.04** (σ^2 = 0.19e^{-3}; P_m = 1)	0.01 (σ^2 = 0.19e^{-3}; P_m = 0.7)	—	—
dlPFC	0.01 (σ^2 = 0.18e^{-3}; P_m = 0.8)	0.01 (σ^2 = 0.19e^{-3}; P_m = 0.78)	0.01 (σ^2 = 0.17e^{-3}; P_m = 0.77)	0 (σ^2 = 0.19e^{-3}; P_m =0.58)	0.01 (σ^2 = 0.19e^{-3}; P_m = 0.86)	—	—
lMC	—	**0.04** (σ^2 = 0.19e^{-3}; P_m = 1)	**0.05** (σ^2 = 0.19e^{-3}; P_m = 1)	**0.04** (σ^2 = 0.19e^{-3}; P_m = 0.99)	**0.03** (σ^2 = 0.19e^{-3}; P_m = 0.98)	**0.03** (σ^2 = 0.2e^{-3}; P_m = 0.99)	0.01 (σ^2 = 0.2e^{-3}; P_m = 0.75)
rMC	—	−0.01 (σ^2 = 0.19e^{-3}; P_m = 0.64)	**−0.02** (σ^2 = 0.19e^{-3}; P_m = 0.96)	**−0.02** (σ^2 = 0.18e^{-3}; P_m = 0.94)	0 (σ^2 = 0.19e^{-3}; P_m = 0.61)	−0.02 (σ^2 = 0.2e^{-3}; P_m = 0.88)	0.01 (σ^2 = 0.2e^{-3}; P_m = 0.69)

Each cell provides statistics for the connection from the column area to the row area. σ^2, sample variance; P, probability that the specified input drives activity in the given region; P_c, probability that the absolute value of the coupling parameter is greater than zero [note that the absolute magnitude of coupling parameters is relative to the driving inputs and will change based on the scale of any parametric modulator (e.g., stimulus value) used as a driving input to the model]; P_m, probability that the coupling parameter is modulated by task condition. The effect size for these parameters should be evaluated relative to the magnitude of the fixed coupling parameters. Parameters with a posterior probability greater than 90% are shown in bold. All values are rounded to two decimals.

Table S9. Modulation of coupling parameters at the time of response

	vmPFC ⇒	*dmPFC* ⇒	*lIPS* ⇒	*rIPS* ⇒	*dlPFC* ⇒	*lMC* ⇒	*rMC* ⇒
vmPFC	—	—	—	—	—	—	—
dmPFC	—	—	—	—	—	—	—
lIPS	—	—	—	—	—	—	—
rIPS	—	—	—	—	—	—	—
dlPFC	—	—	—	—	—	—	—
lMC	—	—	—	—	—	0.01 ($\sigma^2 = 0.2e^{-3}$; $P_m = 0.76$)	0 ($\sigma^2 = 0.2e^{-3}$; $P_m = 0.55$)
rMC	—	—	—	—	—	0 ($\sigma^2 = 0.2e^{-3}$; $P_m = 0.58$)	0.01 ($\sigma^2 = 0.2e^{-3}$; $P_m = 0.76$)

Each cell provides statistics for the connection from the column area to the row area. σ^2, sample variance; *P*, probability that the specified input drives activity in the given region; P_c, probability that the absolute value of the coupling parameter is greater than zero [note that the absolute magnitude of coupling parameters is relative to the driving inputs and will change based on the scale of any parametric modulator (e.g., stimulus value) used as a driving input to the model]; P_m, probability that the coupling parameter is modulated by task condition. The effect size for these parameters should be evaluated relative to the magnitude of the fixed coupling parameters. Parameters with a posterior probability greater than 90% are shown in bold. All values are rounded to two decimals.

Table S10. Parameter estimates for each task related input by region

	Stimulus presentation	Stimulus value	CR left	CR right	Button press
vmPFC	**−0.01** ($\sigma^2 = 0.01e^{-3}$; $P = 0.9$)	**0.04** ($\sigma^2 = 0.23e^{-3}$; $P = 0.99$)	—	—	—
dmPFC	—	—	**0.01** ($\sigma^2 = 0e^{-3}$; $P = 1$)	**0.01** ($\sigma^2 = 0e^{-3}$; $P = 1$)	—
lIPS	—	—	**0.01** ($\sigma^2 = 0e^{-3}$; $P = 1$)	**0.01** ($\sigma^2 = 0e^{-3}$; $P = 1$)	—
rIPS	—	—	**0.01** ($\sigma^2 = 0e^{-3}$; $P = 1$)	**0.01** ($\sigma^2 = 0e^{-3}$; $P = 1$)	—
dlPFC	**−0.01** ($\sigma^2 = 0.01e^{-3}$; $P = 0.99$)	—	**0.01** ($\sigma^2 = 0e^{-3}$; $P = 1$)	**0.01** ($\sigma^2 = 0e^{-3}$; $P = 1$)	—
lMC	—	—	—	—	**0.07** ($\sigma^2 = 0.14e^{-3}$; $P = 1$)
rMC	—	—	—	—	**0.07** ($\sigma^2 = 0.17e^{-3}$; $P = 1$)

Each cell provides statistics for the connection from the column area to the row area. σ^2, sample variance; *P*, probability that the specified input drives activity in the given region; P_c, probability that the absolute value of the coupling parameter is greater than zero [note that the absolute magnitude of coupling parameters is relative to the driving inputs and will change based on the scale of any parametric modulator (e.g., stimulus value) used as a driving input to the model]; P_m, probability that the coupling parameter is modulated by task condition. The effect size for these parameters should be evaluated relative to the magnitude of the fixed coupling parameters. Parameters with a posterior probability greater than 90% are shown in bold. All values are rounded to two decimals.

Table S11. Regions correlated with right and left value across all trials

Region	BA	Side	Cluster size	*x*	*y*	*z*	*Z* score
Region correlated with left value							
Precentral gyrus	3/4	Right	179	48	−19	64	4.15*
Region correlated with right value							
Precentral gyrus	6/4/3	Left	1,073	−42	−19	61	4.88*
Medial frontal gyrus	9/8	Right	176	24	29	37	4.45*
Rolandic operculum/insula	13	Left	149	−42	−28	19	4*
Inferior frontal gyrus	10/46	Right	25	48	53	4	3.67
Middle temporal gyrus	39	Right	21	45	−82	25	3.64
Cerebellum		Right	57	12	−85	−29	3.58
Orbitofrontal cortex	10	Left	37	−21	50	−5	3.51
Occipital cortex	19	Left	20	−12	−97	34	3.09

Height threshold $t = 2.88$; extent threshold = 20 voxels ($3 \times 3 \times 3$ mm). BA, Brodmann area.
*The activation survives whole-brain correction for multiple comparisons at the cluster level (height threshold $t = 2.88$, extent = 178 voxels for the left value, extent = 122 voxels for the right value).